Article

Enhancing Power Quality in Standalone Microgrids Powered by Wind and Battery Systems Using HO Algorithm Based Super Twisting Sliding Mode Controllers

Sana Sahbani [1,*], Oumnia Licer [1], Hassane Mahmoudi [2], Abdennebi Hasnaoui [1] and Mustapha Kchikach [1]

[1] Control and Command of Systems and Renewable Energies (CCSER) Team, (LMTCPS2E) Laboratory, Higher National School of Mines, Rabat P.O. Box 753, Morocco
[2] Electronics Power and Control (EPC) Team, Mohammadia School of Engineers, Mohammed V University, Rabat P.O. Box 765, Morocco
[*] Correspondence: sahbani@enim.ac.ma

Abstract: This paper addresses the challenge of enhancing power quality in a standalone microgrid powered by wind and battery systems. Fluctuations in wind power generation and unpredictable electricity demand significantly impact power quality. To mitigate these issues, a control strategy utilizing Super Twisting Sliding Mode (STSM) controllers tuned by the Hippopotamus Optimization Algorithm (HOA) is proposed. The HOA algorithm efficiently determines optimal STSM controller parameters, leading to improved system performance and stability. A comparative study was conducted against PI, Fuzzy Logic controllers, and other metaheuristic optimization algorithms (PSO, GWO, WOA). Simulation results, obtained using MATLAB/Simulink, demonstrate the superior performance of the proposed methodology. Specifically, during a simulated abrupt load change, the system exhibited rapid recovery with frequency reaching equilibrium, significantly faster than PI and Fuzzy Logic controllers. Moreover, the DC link voltage remained stable with fluctuations of only 2%, while the three-phase RMS voltages at the Point of Load Bus (PLB) maintained balanced and stable values. These results confirm the enhanced power quality and robust operation achieved with the proposed HOA-tuned STSM control strategy, outperforming other tested methods. The methodology effectively manages both the energy management system and improves power quality in standalone wind and battery-powered microgrids.

Keywords: wind system; battery storage; power quality; microgrid; super twisting sliding mode controllers; HOA

1. Introduction

The challenges posed by climate change highlight the urgent need for a global shift towards renewable energy sources. This transition is essential to meet the increasing electricity demand while addressing the depletion of natural resources, global warming, and rising electricity costs, thereby decreasing reliance on fossil fuels and minimizing carbon emissions [1].

The utilization of wind energy has become increasingly favored, particularly because of its plentiful nature and sustainable characteristics [2,3]. Therefore, the implementation of Standalone Microgrid Systems (SMSs) can address numerous challenges, such as delivering electricity to consumers, minimizing pollution, and ensuring a reliable and stable power supply. These SMSs can utilize wind energy by employing small-scale wind turbines, which produce electricity that is subsequently stored in batteries for later use [4]. This technology proves to be especially beneficial in remote or off-grid locations where conventional power sources might be inconsistent or inaccessible. The quality of electricity generated by the Wind Power Conversion System (WPCS) can fluctuate significantly based on the wind speed at any particular time. In conditions of strong winds, the system is capable of

producing a substantial amount of power; however, during periods of calm winds, the power output may be minimal or nonexistent. The inconsistency inherent in wind power presents difficulties in depending exclusively on it for stable energy generation, as it does not serve as a constant and dependable energy source. To address this challenge, WPCSs are frequently integrated with energy storage systems, such as Battery Storage Units (BSUs), to provide a more reliable and steady power supply [5–8].

In the WPCS-BSU system, power quality is affected by fluctuations in electricity production due to the variability of weather conditions and unpredictability in electricity demand [9]. In this context, power quality pertains to the attributes of the electricity supply, encompassing voltage stability, frequency control, and the absence of disturbances or interruptions [10]. Thus, to maintain overall system reliability and efficiency, power electronics and their control systems play a significant role in enabling the system to produce maximum power despite internal or external variations. Additionally, they are used not only to manage power flow to ensure equilibrium within electrical systems but also to manage frequency, voltage, and the control of active and reactive power, as well as to address harmonics [11,12].

Many different structures and control algorithms have been developed to control power quality. Proportional-integral (PI) control is widely used in various applications, including wind energy systems, due to its simplicity but is not sensitive to external or internal variations, such as wind speed turbulence and the changes in wind system parameters, that can significantly degrade system performance [13]. For this reason, nonlinear controls have been developed to be less sensitive to wind speed and parameter variations. In this context, Fuzzy Logic Control (FLC) provides better performance in managing nonlinearities and uncertainties in wind energy systems. However, its complexity in design and reliance on well-defined rules can be challenging [14]. A sliding mode controller (SMC) has a better control response, in comparison with the other strategies, by providing a more robust response to external disturbances [15–17]. However, it can suffer from chattering effects, which may lead to a reduction in overall system efficiency. In response to these limitations, the Super Twisting Sliding Mode Controller (STSMC) has been developed to enhance performance by mitigating chattering while maintaining robust control. The STSMC operates by using a continuous control approach, which smooths out the control actions and reduces wear on system components. This advantage makes it particularly effective in (SMS) powered by (WPCS) and (BSU) [18,19]. However, to optimize the performance of the (STSM) Controller, particularly in handling the dynamic and nonlinear behavior of such systems, there is a pressing need for properly tuned parameters.

To achieve optimal performance, it is crucial to fine-tune its parameters effectively. Combining the STSMC with a metaheuristic algorithm provides powerful tools for solving complex optimization problems under various operating conditions [20,21]. A metaheuristic is an algorithm designed to solve approximately a wide range of hard optimization problems without having to adapt deeply to each problem; they are nature-inspired and based on some principles from physics, biology, or ethology [22]. Specifically, the swarm intelligence algorithm simulates the behavior of a biological population or natural phenomena, and a group of simple individuals follows specific interaction mechanisms to complete a given complex optimization problem involving continuous and discrete variables, as well as multi-dimensional and nonlinear challenges. Swarm intelligence algorithms exhibit advantages such as robustness and economy [23].

Many swarm intelligence algorithms have emerged. Ref. [24] Introduces Particle Swarm Optimization (PSO), inspired by the regularity of bird flocking behavior. The Whale Optimization Algorithm (WOA) simulates the behaviors of whale swarming, including encircling, pursuing, and attacking prey, to achieve optimization objectives [25,26]. The Grey Wolf Optimization (GWO) Algorithm is inspired by the hunting behaviors of wolf packs as they search for prey [27]. The Hippopotamus Optimization Algorithm (HOA) simulates defense and evasion strategies against predators while performing location updates. It boasts advantages such as high accuracy, strong local search capability, and good practicality [28].

To achieve the optimal response of the studied microgrid control systems, the HOA will be developed to estimate appropriate parameters for the various STSM controllers discussed in this paper. The organization of the paper is as follows: Section 2 provides a detailed description of the topic, while Section 3 outlines the process for estimating the parameters of STSM controllers using HOA. Sections 4 and 5 present the detailed mathematical modeling and proposed methodology, respectively. Section 6 includes a small signal analysis of the system. Various results obtained from simulations are discussed in Section 7. Finally, the conclusion and references are presented at the end of the paper.

2. Standalone Microgrid System

Figure 1 illustrates the general topology of the designed SMS; it consists of the main following components: The WPCS includes a wind turbine that converts the kinetic energy of the wind into electrical energy. This electrical energy is then transformed from alternating current (AC) to direct current (DC) through a rectifier, ensuring compatibility with the DC link. The DC link serves as a pivotal connection, allowing the WPCS to convey the energy it generates to the BSU. The BSU is essential to the system as it retains surplus energy produced by the wind turbine, which is utilized during periods of low wind or high demand.
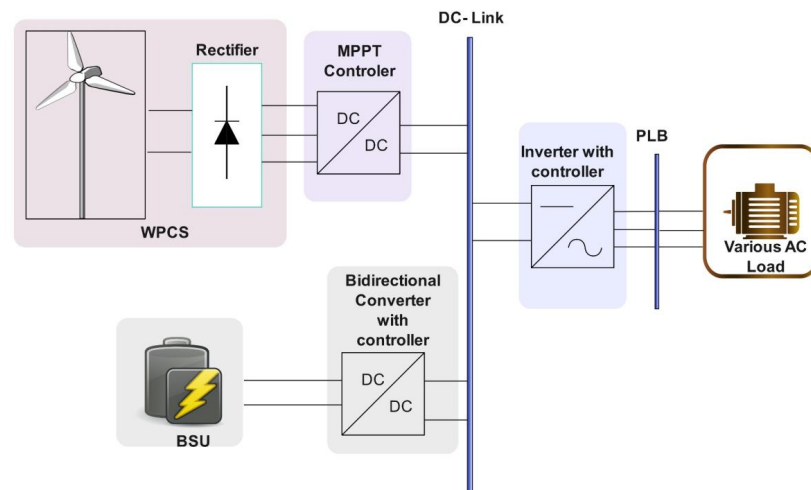

Figure 1. Standalone microgrid supplied by WPCS-BSU.

Additionally, the BSU is connected to the DC link via a bidirectional converter, facilitating flexible energy transfer between the WPCS and the BSU. An inverter is linked to the DC link to supply power to AC loads, converting the stored DC power into AC power suitable for residential or industrial applications. This enables the use of energy stored in the BSU or generated by the wind turbine to support both three-phase and single-phase AC loads at the Point of Load Bus (PLB), enhancing the overall efficiency and reliability of the renewable energy system.

3. HOA-Based STSM Controller

Sliding mode control is a highly regarded control strategy that has received considerable acknowledgment in the context of various nonlinear systems [19,20]. The STSM controller is capable of resolving the chattering problems typically linked to conventional sliding mode control, thereby facilitating smooth control [29]. The control law for this nonlinear system is articulated in the following way.

$$
\begin{cases}
u = a_2|e|^{\frac{1}{2}}\mathrm{sgn}(e) + v \\
\dot{v} = a_3\mathrm{sgn}(e)
\end{cases}
\tag{1}
$$

where a_2 and a_3 are gains, $e = a_1$(input-reference) + differentiation of (input-reference), and v is the sliding surface. Hence:

$$output = a_2\sqrt{e}\text{sgn}(e) + \int a_3\text{sgn}(e)dt \tag{2}$$

Figure 2 illustrates the block diagram of the STSM control system. The adjustment of variables a_1, a_2, and a_3 presents significant challenges when employing multiple STSM controllers within the proposed control model. Consequently, the PSO method [30] is employed to estimate different parameters within the STSM controller. However, HOA has a higher significance priority than PSO to identify the best solution [27]. In the process of developing the algorithm for the adaptive STSM controller, which involves the selection of design parameter values for the sliding mode control algorithm, an HOA approach is utilized and executed by Equations (3)–(20).
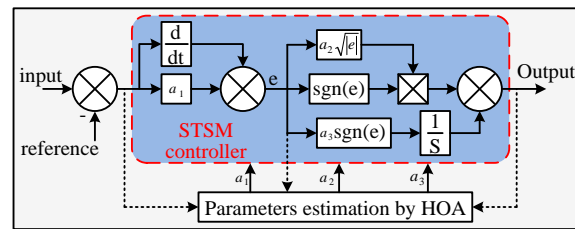

Figure 2. Symmetric diagram of STSM controller.

The function $f(x)$ is influenced by the position of the STSM controller utilized in the proposed control methodology:

$$f = \int_0^T t(|input - reference|)dt \tag{3}$$

The HOA algorithm is a population-based optimization method that represents basic mathematical equations using the following expressions:

$$H_i = B_j^L + k \times \left(B_j^U - B_j^L\right); \; i = 1, 2, \ldots N; \; j = 1, 2, 3 \ldots M \tag{4}$$

$$H = \begin{bmatrix} H_1 \\ \vdots \\ H_i \\ \vdots \\ H_N \end{bmatrix}_{N \times M} = \begin{bmatrix} h_{1,1} & \cdots & h_{1,j} & \cdots & h_{1,M} \\ \vdots & \ddots & \vdots & \ddots & \vdots \\ h_{i,1} & \cdots & h_{i,j} & \cdots & h_{i,M} \\ \vdots & \ddots & \vdots & \ddots & \vdots \\ h_{N,1} & \cdots & h_{N,j} & \cdots & h_{N,M} \end{bmatrix}_{N \times M} \tag{5}$$

The hippopotamus group has three behavioral procedures, as outlined previously, which are mathematically represented in the equations below:

Behavior-1: The current location of the hippos in the river or pond has been revised (Exploration): The leading Hippopotamus is ascertained through the objective function value iteration. Normally, hippos have a tendency to congregate near each other. The dominant male hippos take on the role of protecting the herd and their territory from potential threats. Several female hippos are situated near the male hippos. The male hippopotamus members positions within the lake or pond can be mathematically represented by the following equations:

$$H_i^{male} = h_{ij} + a_1 \cdot \left(D_h - a_2^{ij}\right) \tag{6}$$

$$b = \begin{cases} a_3 \times \vec{k}_1 + (\approx \delta_1) \\ 2 \times \vec{k}_2 - 1 \\ \vec{k}_3 \\ a_2 \times \vec{k}_4 + (\approx \delta_1) \\ \vec{k}_5 \end{cases} \tag{7}$$

$$H_i^{female} = \begin{cases} h_{ij} + b_1 \cdot \left(D_h - a_3^{ij} \cdot R_i \right) \exp\left(\frac{-t}{\tau} \right) > 0.6, \; else \\ h_{ij} + b_2 \cdot (R_i - D_h) k_6 > 0.5, \; else \\ B_j^L + k_7 \left(B_j^U - B_j^L \right) \end{cases} \tag{8}$$

$$H_i = \begin{cases} H_i^{male} \times F_i^{male} < F_i; \; else \\ H_i \end{cases} \tag{9}$$

$$H_i = \begin{cases} H_i^{female} \times F_i^{female} < F_i; \; else \\ H_i \end{cases} \tag{10}$$

Behavior-2: Defense system of Hippopotamus against predators: The safety and security of hippopotamuses is a major contributing factor to their tendency to live in herds. Hippopotamuses primarily defend themselves by quickly turning towards the predator and emitting loud vocalizations to discourage the predator from getting too close. At this stage, Hippopotamuses may demonstrate a behavior of approaching the predator in order to make it retreat, effectively fending off the potential threat. Equations provided illustrate the location of the predator within the search space:

$$P_j = B_j^L + \vec{k}_8 \left(B_j^U - B_j^U \right); \; j = 1, 2 \ldots\ldots M \tag{11}$$

$$\vec{G} = |P_j - H_{i,j}| \tag{12}$$

In this instance, the Hippopotamus shifts its position toward the predator, albeit with a restricted range of motion. The aim is to alert the predator or intruder to its presence in its territory:

$$H_i^P = \begin{cases} \vec{R}_L \oplus P_j + \left(\frac{f}{\lambda \times \cos(2\pi j)} \right) \cdot \frac{F_{P_j}}{\vec{G}} < F_i \\ \vec{R}_L \oplus P_j + \left(\frac{f}{\lambda \times \cos(2\pi j)} \right) \cdot \frac{F_{P_j}}{2 \times \vec{G} + \vec{k}_9} \geq F_i \end{cases} \tag{13}$$

$$H_i = \begin{cases} H_i^{P_j} \times F_i^{P_j} < F_i \\ H_i \times F_i^{P_j} \geq F_i \end{cases} \tag{14}$$

The Levy distribution is employed to account for abrupt shifts in the predator's location when launching an attack on the Hippopotamus. The mathematical formula for the stochastic motion of Lévy movement is derived as follows:

$$Levy(\eta) = \frac{0.05 \times \omega \times \left[\frac{\Gamma(1+\eta) \sin\left(\frac{\pi\eta}{2} \right)}{\Gamma\left(\frac{1+\eta}{2} \right) \eta \times 2^{\frac{\eta-1}{2}}} \right]^{\frac{1}{\eta}}}{|\eta|^{\frac{1}{\eta}}} \tag{15}$$

Behavior-3: Escaping the nature of the Hippopotamus from the Predator: The Hippopotamus exhibits a different behavior when faced with a predator, such as when it encounters a group of predators or is unable to fend off the predator using its defensive tactics. The approach results in the Hippopotamus discovering a secure spot near its present whereabouts, and incorporating this conduct during the third behavior of the HOA improves its capacity for local search exploitation:

$$_{local}B_j^L = \frac{B_j^L}{\gamma}; \; _{local}B_j^U = \frac{B_j^U}{\gamma}; \; \gamma - 1, 2, \ldots \tau \tag{16}$$

$$H_i^{E_j} = H_{ij} + k_{10} \left(_{local}B_j^L + \psi \left(_{local}B_j^U - _{local}B_j^L \right) \right) \tag{17}$$

$$\psi = \begin{cases} 2 \times \vec{k}_{11} - 1 \\ k_{12} \\ k_{13} \end{cases} \tag{18}$$

$$H_i = \begin{cases} H_i^{E_j} \times F_i^{E_j} < F_i \\ H_i \times F_i^{E_j} \geq F_i \end{cases} \tag{19}$$

The best solution of the above procedure from behavior 1 to 3 can be replaced as the best error signal (*e*) by the below expression:

$$e_i = \begin{cases} H_i \times F_i & < \xi;\ else; \\ H_i, \end{cases} \tag{20}$$

The procedure will continue to be executed until the optimal values of a_i are achieved. The respective flowchart of the proposed algorithm is shown in Figure 3.
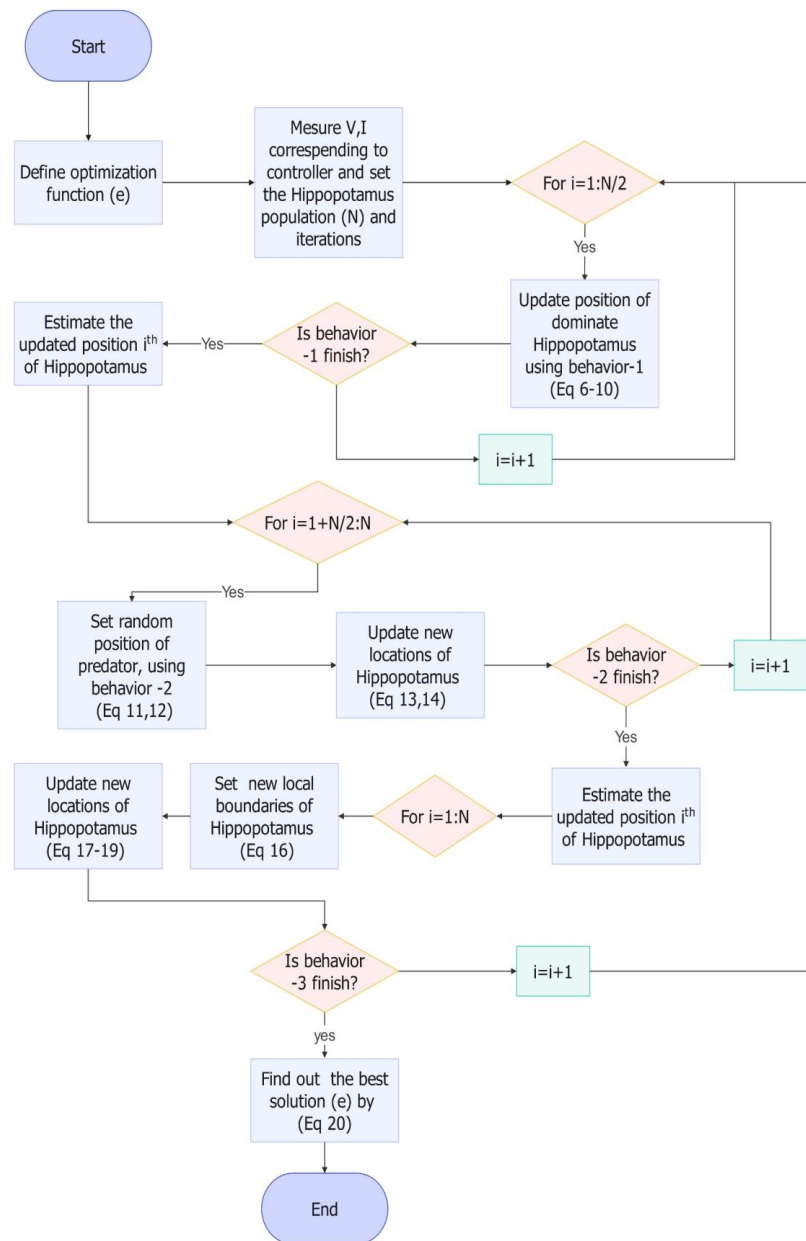
Figure 3. Flowchart of HOA for 'e'.

4. Mathematical Modeling of STSM-Based Proposed System

Considered internal parameters of the microgrid are shown in Table 1 as follows:

Table 1. Microgrid Parameters Notations.

Microgrid Parameters	Notations
Internal resistance of wind MPPT (boost converter)	Rw
Inductor of wind MPPT	Lw
Duty cycle of MPPT	Dw
Input voltage of MPPT	Vw
Current flowing through MPPT	Iw
Battery voltage	Vb
Inductor of bidirectional converter	Lb
Resistance of bidirectional converter	Rb
Duty cycle of bidirectional converter	D
Current flowing through bidirectional converter	Ib
Output voltage (DC link voltage)	Vdc

The generalized layout of the wind-battery system with only their respective converters is shown in Figure 4.
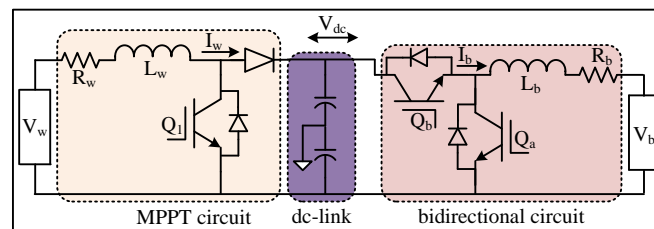
Figure 4. Generalized layout of wind-battery with their respective converters.

The following basic equations are obtained by using KVL law:

$$V_w = L_w \frac{dI_w}{dt} + R_w I_w + (1 - D_w)V_{dc} \tag{21}$$

$$V_b = L_b \frac{dI_b}{dt} + R_b I_b + (1 - D)V_{dc} \tag{22}$$

However, the battery current is in bidirectional flow, and also the duty cycle can be represented by:

$$D = \begin{cases} 1 & if \ I_b > 0; \quad Q_b \ ON \\ 0 & if \ I_b < 0; \quad Q_a \ ON \end{cases} \tag{23}$$

In an ideal case, input and output powers must be balanced; hence:

$$P_w + P_{bat} = P_{load} \tag{24}$$

$$V_w I_{w,ref} + V_b I_{b,ref} = V_{dc} I_{dc,ref} \tag{25}$$

Hence:

$$I_{dc,ref} = \lambda \frac{\left(V_w I_{w,ref} + V_b I_{b,ref}\right)}{V_{dc}} \tag{26}$$

where 'λ' is the ideality factor, which shows the power converter's losses.

Considering errors of the system by (main errors signals of DC side controllers).

$$e_1 = I_w - I_{w,ref} \tag{27}$$

$$e_2 = I_b - I_{b,ref} \tag{28}$$

A similar analysis is also conducted for other STSM controllers.

The change in error is also considered,

$$\dot{e}_1 = \dot{I}_w - \dot{I}_{w,ref} \tag{29}$$

$$\dot{e}_2 = \dot{I}_b - \dot{I}_{b,ref} \tag{30}$$

Therefore:

$$\dot{e}_1 = \frac{V_w}{L_w} - \frac{R_w}{L_w}I_w - \frac{(1-D_w)}{L_w}V_{dc} - \dot{I}_{w,ref} \tag{31}$$

$$\dot{e}_2 = \frac{V_b}{L_b} - \frac{R_b}{L_b}I_b - \frac{(1-D)}{L_b}V_{dc} - \dot{I}_{b,ref} \tag{32}$$

A similar approach is also conducted for other STSM controllers based on their error signals.

5. Proposed Control Methodologies

5.1. MPPT Control of WPCS

Figure 5 presents a diagrammatic representation of the proposed control strategy for the MPPT of WPCS.
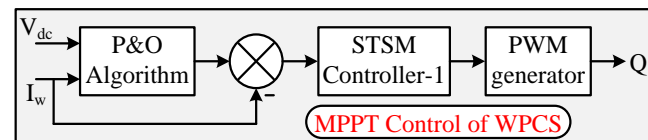
Figure 5. Proposed MPPT control of WPCS.

The wind turbine's speed signal, essential for the effective execution of MPPT in WPCS [5], is frequently difficult to acquire and susceptible to errors in current methodologies. Therefore, a P&O method is employed that necessitates only voltage and current signals, which are derived from the DC link and the current injected into the DC link from the WPSC (i.e., Iw). To minimize the number of sensors required, the approach is executed by focusing on the voltage at the DC link (i.e., Vdc) rather than the voltage across the three-phase diode rectifier. The application of the P&O algorithm enables the system to follow the reference current, which varies with wind speed, to optimize power generation. The P&O approach for WPCS is derived from the fundamental equation presented below [31]:

$$I_w^{k+1} = I_w^k + \Delta I_w \times sign\left(\frac{dP_w}{dI_w}\right) \tag{33}$$

The output signal generated by the P&O algorithm is subsequently compared with the actual wind current (Iw). The HOA-STSM controller-1 will receive the error signal to produce the necessary pulses for switch Q1, which is utilized in the MPPT circuit of the WPCS.

5.2. Control of Bidirectional Circuit

The bidirectional DC–DC converter control system (Figure 6) employs a multi-loop architecture incorporating STSM controllers to manage efficient and safe energy transfer between the BSU and the external power source or load. The system's operation is heavily dependent on the switching states of transistors Qa and Qb, which determine the direction and magnitude of current flow. A crucial element is the consideration of the battery's state of charge (SoC) to prevent overcharging or excessive discharge. An "estimating oscillating component" block enhances robustness by compensating for voltage fluctuations. Three STSM controllers work in tandem, utilizing feedback from battery current (Ib) and DC link voltage (Vdc) to precisely regulate the charging and discharging currents while considering

the SoC. These controllers generate PWM signals to control the converter's switches, ensuring optimal energy management and system stability.
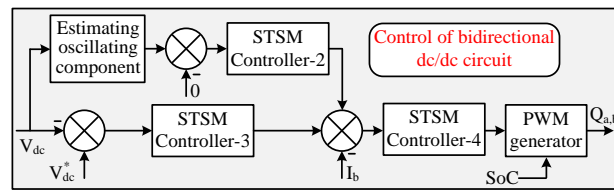

Figure 6. Control method of the bidirectional DC/DC circuit.

5.3. Control of Inverter

Figure 7 depicts the proposed control strategy for the three-phase inverter within the standalone microgrid. The system continuously monitors the RMS voltage (Vrms) and frequency (F) at the Point of Load Bus (PLB), comparing these measurements to their desired setpoints. Any deviation results in error signals that are processed by super-twisting sliding mode (STSM) controllers (Controllers 5 and 6). These controllers generate reference direct (idc*) and quadrature (iq*) currents, which are used to regulate the actual direct (idc) and quadrature (iq) currents flowing in the inverter. This regulation is achieved by manipulating the Sinusoidal Pulse Width Modulation (SPWM) signals (P1–P6) supplied to the inverter's switching elements. This control approach employs the robust nature of STSM controllers to ensure accurate tracking of the desired voltage and frequency at the PLB, maintaining stable system operation despite variations in load and renewable energy generation. The rapid response of the controllers makes the system resilient to dynamic changes inherent in microgrids with renewable energy sources.
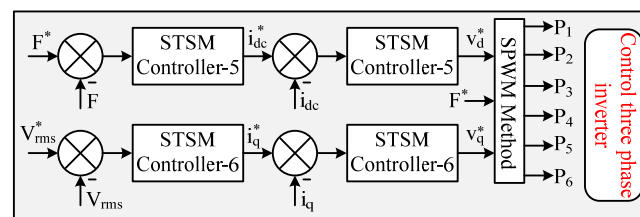

Figure 7. Proposed control of the inverter.

6. Simulation Results

Figure 8 shows the overall system design of the studied standalone microgrid (SMS), implemented in MATLAB/Simulink. Various input signals from sensors (shown in green) are used by the controllers. These signals are converted to digital form and sent as output signals to the converters (shown in red). This section presents the results of a series of tests.
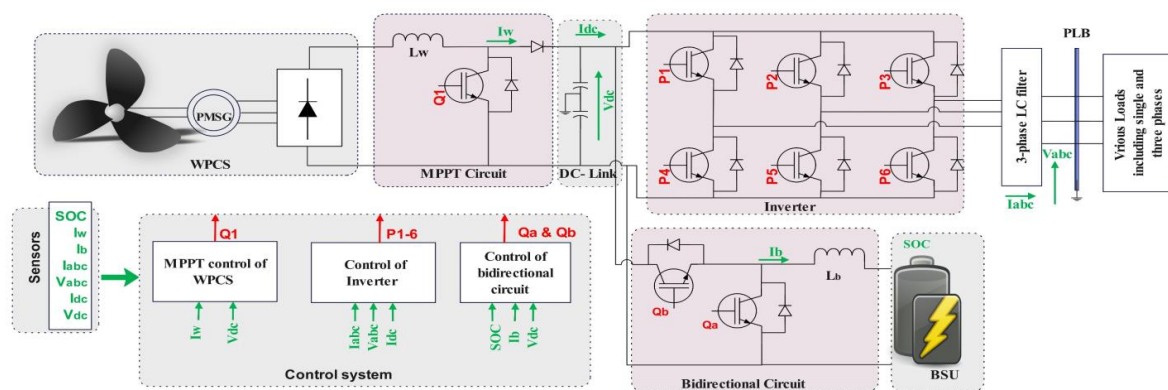

Figure 8. Detailed configuration of the SMS studied.

6.1. Comparison of STSM with PI and FLC Controllers

The SMS undergoes testing at a load variation of 200% at PLB, utilizing STSM, Fuzzy, and PI controllers. The load is introduced at 1.5 s and removed at 1.65 s. Throughout this time frame, an analysis of the frequency response among STSM, Fuzzy, and PI controllers is conducted and illustrated in Figure 9 with a zoomed-in view. The frequency response achieved with the STSM controllers is stable and reaches equilibrium rapidly in comparison with the other controllers. Consequently, additional tests are performed utilizing the proposed control strategy with STSM controllers.
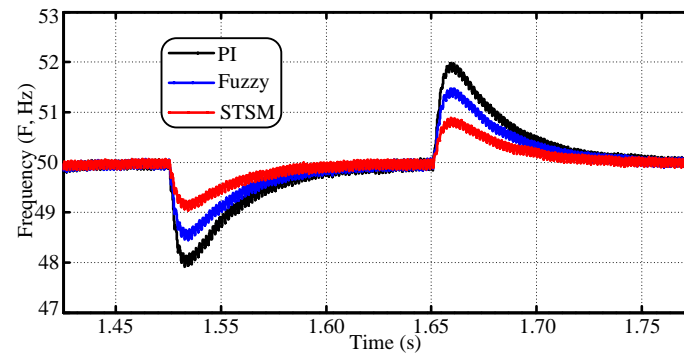
Figure 9. Response of frequency with STSM, Fuzzy, and PI controller.

6.2. Response Under Load Change

A complete change in load is observed at t = 1.5 s, with the release occurring at t = 2 s. Throughout this timeframe, the proposed control methodology effectively stabilized the voltages at both the DC link and the Power Load Balance (PLB). Figure 10a presents a zoomed-in view of the voltage at the DC link, showcasing small fluctuations of approximately 2%. This minor variability highlights the effectiveness of the developed energy management system (EMS) through the proposed control methodology.
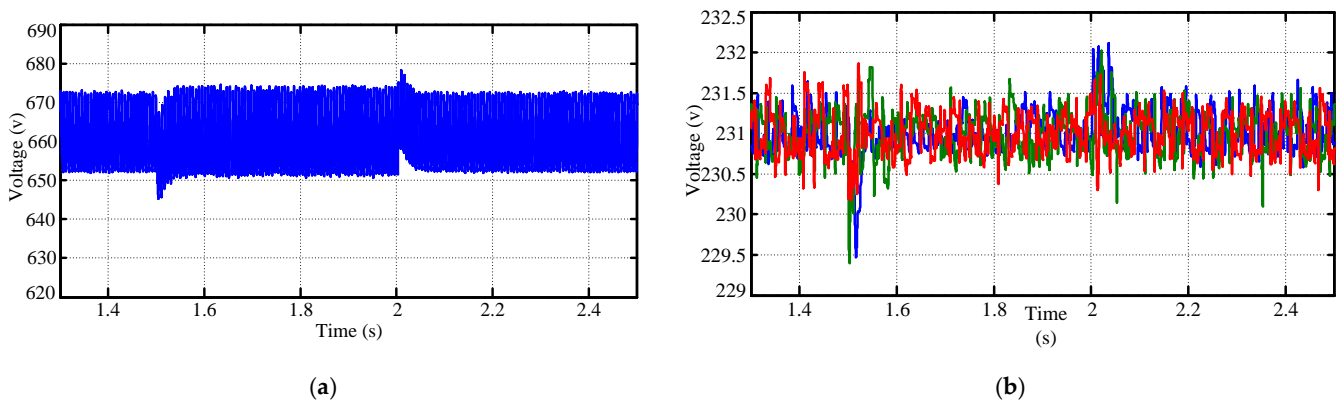

(a)

(b)

Figure 10. (**a**) Response of voltage at DC link; (**b**) Three phase RMS voltages at PLB.

The graph in Figure 10b offers a detailed perception of the three-phase RMS voltages at the PLB, particularly during a dynamic load event. While the overall voltage levels remain within the nominal operating range, this zoomed-in view reveals rapid fluctuations in the RMS voltage of each phase during the transient load event (1.5–2 s). Although these fluctuations are more pronounced during the load change, the system demonstrates a quick recovery, maintaining stability within a remarkably small fluctuation range.

6.3. Response Under Change in Wind Speed

The SMS response is evaluated in relation to variations in wind speed. The wind speed is altered at t = 2.0 s, while the load is simultaneously increased at t = 1.75 s. In

the event of a variation in wind speed, the suggested control methodology for MPPT effectively monitors the maximum power, as illustrated in Figure 11a, which also presents the response of torques. Therefore, the proposed control of MPPT depicted in Figure 5 is working effectively under rapid changes in wind speed. The respective powers of the load, BSU, and WPCS are illustrated in Figure 11b. From this figure, it is observed that the EMS helps the BSU to respond according to the power balance between generation and load at the PLB.

(a)　　　　　　　　　　　　　　　(b)
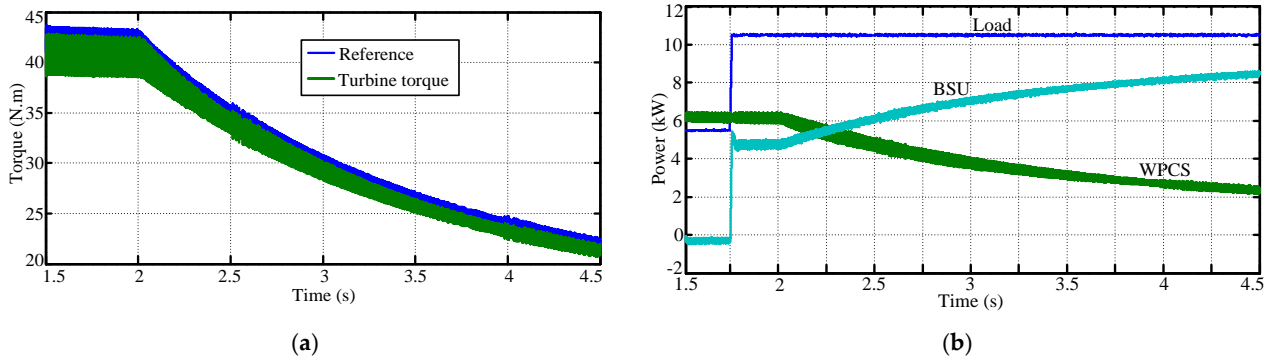
Figure 11. (**a**) Response of torque of WPCS; (**b**) various powers in SMS.

6.4. Performance of HOA

The response of the error signal from Vrms is considered for comparison among proposed HOA-STSM, PSO-STSM, STSM (simple tuned STSM control), and the conventional PI controller. A step change of 75% load is applied at t = 7.50 s at PLB for testing in this case. The error signal response (expressed as a percentage of the normalized value derived from the equation below) is illustrated in Figure 12. By observing this figure, the response has improved by using the proposed method with HOA. Error is very nominal in the case of optimized parameters by using HOA.

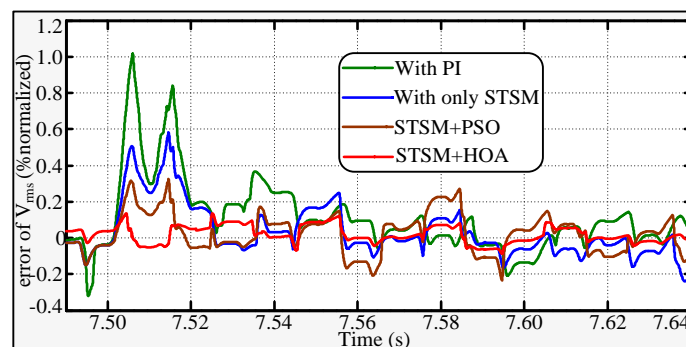$$\% \text{ of normalized } V_{rms} = \frac{V_{rms}^* - V_{rms}}{V_{rms}^*} \times 100 \tag{34}$$

Figure 12. Response of error signal.

6.5. Convergence with HOA

Various parameters of the STSM controller are obtained by using Grey Wolf Optimization (GWO), Whale Optimization Algorithm (WOA), and HOA. The convergence of the respective algorithms is depicted in Figure 13, and it was found that the HOA had the best response as compared with others. This implies the response of the controller is improved by the proposed STSM-HOA method.
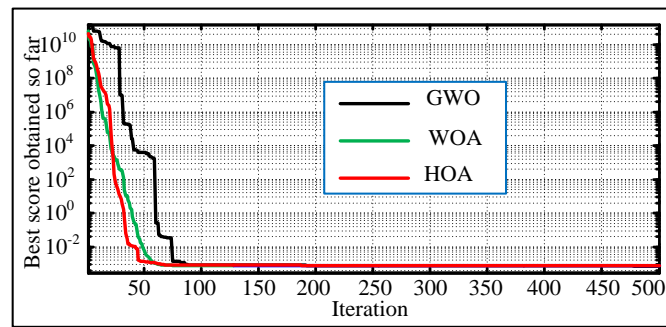
Figure 13. Convergence of HOA over GWO and WOA.

6.6. Responses with Small Change in Reference

Response for small changes in reference to the Vdc is also carried out. Small changes for decreasing and increasing change in Vdc are applied at t = 3.0 and 4.0 s. The corresponding response for the actual DC link voltage is depicted in Figure 14. It can be seen that a stable response is observed, and the actual DC link voltage is fast enough to follow its reference value.
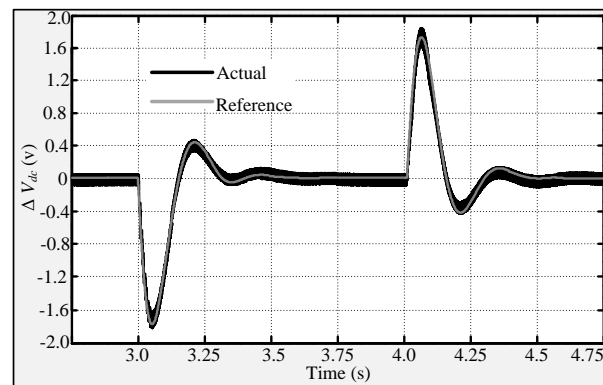

Figure 14. Response of change in DC link voltage.

7. Conclusions

This study presented a novel control strategy for enhancing power quality in a standalone microgrid powered by wind and battery systems. The proposed approach employed Super-Twisting Sliding Mode Controllers with parameters optimized using the Hippopotamus Optimization Algorithm. Simulation results, obtained using MATLAB/Simulink, demonstrated the effectiveness of this method in maintaining stable DC link voltage and balanced three-phase RMS voltages at the Point of Load Bus, even under significant load variations. A comparative analysis against PI, Fuzzy Logic controllers, and other meta-heuristic algorithms (PSO, GWO, WOA) revealed the superior performance of the proposed HOA-STSMC approach in terms of speed of response and stability. This superior performance was attributed to the HOA's efficient parameter optimization and the STSMC's inherent robustness to disturbances.

Future work will focus on several key areas; a comprehensive small-signal stability analysis will be conducted to rigorously assess the system's dynamic behavior and stability margins under various operating conditions. Moreover, exploring different metaheuristic algorithms and their potential for improving parameter optimization for various load profiles will be investigated to further enhance the performance and robustness of the proposed control methodology.

References

1. Sahbani, S.; Mahmoudi, H.; Hasnaoui, A.; Kchikach, M. Development prospect of smart grid in Morocco. *Procedia Comput. Sci.* **2016**, *83*, 1313–1320. [CrossRef]
2. Zhang, H.; Chen, Y.; Gao, Y.; Zhao, M.; Wang, H.; Lei, Z. Research on Energy Conversion Benefits of Hybrid Wind Power and Concentrating Solar Power System Based on Time-of-use Electricity Price. In Proceedings of the 2023 24th International Conference on Electronic Packaging Technology (ICEPT), Shihezi City, China, 8–11 August 2023; pp. 1–5.
3. Akbari, R.; Izadian, A. Reduced-size converter in dfig-based wind energy conversion system. In Proceedings of the 2020 IEEE Energy Conversion Congress and Exposition (ECCE), Detroit, MI, USA, 11–15 October 2020; pp. 4217–4223.
4. Kumar, P.; Palwalia, D.K. Feasibility study of standalone hybrid wind-PV-battery microgrid operation. *Technol. Econ. Smart Grids Sustain. Energy* **2018**, *3*, 17. [CrossRef]
5. Badawi, A.S.; Hasbullah, N.F.; Yusoff, S.H.; Hashim, A.; Khan, S.; Zyoud, A.M. Paper review: Maximum power point tracking for wind energy conversion system. In Proceedings of the 2020 2nd International Conference on Electrical, Control and Instrumentation Engineering (ICECIE), Kuala Lumpur, Malaysia, 28 November 2020; pp. 1–6.
6. Gao, Q.; Ertugrul, N.; Ding, B.; Negnevitsky, M. Offshore wind, wave and integrated energy conversion systems: A review and future. In Proceedings of the 2020 Australasian Universities Power Engineering Conference (AUPEC), Hobart, Australia, 29 November 2020; pp. 1–6.
7. Chen, W.; Yang, W.; Chen, Q.; Li, J.; Geng, H. Wind Speed Estimation for PMSG-Based WECS under Power Limit Control. In Proceedings of the 2023 IEEE 6th International Electrical and Energy Conference (CIEEC), Hefei, China, 12–14 May 2023; pp. 1288–1292.
8. dos Santos, Â.M.M.; Pacífico, R.P.; Costa, N.S.; de França, M.V.; Teixeira, V.S.D.C.; Moreira, A.B. Control of SCIG Based on Wind Energy Conversion System with BESS. In Proceedings of the 2023 IEEE 8th Southern Power Electronics Conference (SPEC), Florianopolis, Brazil, 26–29 November 2023; pp. 1–7.
9. Su, W.; Wang, J. Energy management systems in microgrid operations. *Electr. J.* **2012**, *25*, 45–60. [CrossRef]
10. Alkahtani, A.A.; Alfalahi, S.T.; Athamneh, A.A.; Al-Shetwi, A.Q.; Mansor, M.B.; Hannan, M.A.; Agelidis, V.G. Power quality in microgrids including supraharmonics: Issues, standards, and mitigations. *IEEE Access* **2020**, *8*, 127104–127122. [CrossRef]
11. Chen, Z.; Guerrero, J.M.; Blaabjerg, F. A Review of the state of the art of power electronics for Wind turbines. *IEEE Trans. Power Electron.* **2009**, *24*, 1859–1875. [CrossRef]
12. Ali, T.; Malik, S.A.; Daraz, A.; Adeel, M.; Aslam, S.; Herodotou, H. Load Frequency Control and Automatic Voltage Regulation in Four-Area Interconnected Power Systems Using a Gradient-Based Optimizer. *Energies* **2023**, *16*, 2086. [CrossRef]
13. Krim, Y.; Abbes, D.; Krim, S.; Mimouni, M.F. Classical vector, first-order sliding mode and high-order sliding-mode control for a grid-connected variable speed wind energy conversion system: A comparative study. *Wind Eng.* **2018**, *42*, 16–37. [CrossRef]
14. Zamzoum, O.; Derouich, A.; Motahhir, S.; El Mourabit, Y.; El Ghzizal, A. Performance analysis of a robust adaptive fuzzy logic controller for wind turbine power limitation. *J. Clean. Prod.* **2020**, *265*, 121659. [CrossRef]
15. Belaimeche, F.Z.; Bentaallah, A.; Massoum, S.; Wira, P. A comparative study between a simplified fuzzy PI and classic PI input-output linearizing controller for the wind-turbine doubly fed induction generator. *Elektrotehniški Vestn. J. Electr. Eng. Comput. Sci.* **2018**, *85*, 142–148.
16. Serhoud, H.; Benattous, D. Sliding mode control of brushless doubly-fed machine used in wind energy conversion system. *Rev. Des Energ. Renouvelables* **2012**, *15*, 305–320. [CrossRef]
17. Bouguerra, Z. Comparative study between PI, FLC, SMC and Fuzzy sliding mode controllers of DFIG wind turbine. *J. Renew. Energ.* **2023**, *26*, 209–223. [CrossRef]
18. Yang, W.; Han, Y.; Ma, R.; Hou, M.; Yang, G. A composite super-twisting sliding mode approach for platform motion suppression and power regulation of floating offshore wind turbine. *J. Mar. Sci. Eng.* **2023**, *11*, 2318. [CrossRef]
19. Utkin, V. Sliding mode control of DC/DC converters. *J. Frankl. Inst.* **2013**, *350*, 2146–2165. [CrossRef]
20. Rezoug, A.; Messah, A.; Messaoud, W.A.; Baizid, K.; Iqbal, J. Adaptive-optimal MIMO nonsingular terminal sliding mode control of twin-rotor helicopter system: Meta-heuristics and super-twisting based control approach. *J. Braz. Soc. Mech. Sci. Eng.* **2024**, *46*, 162. [CrossRef]
21. Mohapatra, B.; Sahu, B.K.; Pati, S.; Bajaj, M.; Blazek, V.; Prokop, L.; Misak, S. Optimizing grid-connected PV systems with novel super-twisting sliding mode controllers for real-time power management. *Sci. Rep.* **2024**, *14*, 4646. [CrossRef]

22. Abd Elaziz, M.; Dahou, A.; Abualigah, L.; Yu, L.; Alshinwan, M.; Khasawneh, A.M.; Lu, S. Advanced metaheuristic optimization techniques in applications of deep neural networks: A review. *Neural Comput. Appl.* **2021**, *33*, 14079–14099. [CrossRef]

23. Tang, J.; Liu, G.; Pan, Q. A review on representative swarm intelligence algorithms for solving optimization problems: Applications and trends. *IEEE/CAA J. Autom. Sin.* **2021**, *8*, 1627–1643. [CrossRef]

24. Kennedy, J.; Eberhart, R. Particle swarm optimization. In Proceedings of the ICNN'95-International Conference on Neural Networks, Perth, WA, Australia, 27 November 1995; Volume 4, pp. 1942–1948.

25. Mirjalili, S.; Lewis, A. The whale optimization algorithm. *Adv. Eng. Softw.* **2016**, *95*, 51–67. [CrossRef]

26. Deepak, K.; Mandal, R.K.; Verma, V. Improvement of power quality by using novel controller for hybrid renewable energy sources based microgrid. *Int. J. Emerg. Electr. Power Syst.* **2024**, *25*, 289–303. [CrossRef]

27. Dada, E.; Joseph, S.; Oyewola, D.; Fadele, A.A.; Chiroma, H. Application of grey wolf optimization algorithm: Recent trends, issues, and possible horizons. *Gazi Univ. J. Sci.* **2022**, *35*, 485–504. [CrossRef]

28. Amiri, M.H.; Mehrabi Hashjin, N.; Montazeri, M.; Mirjalili, S.; Khodadadi, N. Hippopotamus optimization algorithm: A novel nature-inspired optimization algorithm. *Sci. Rep.* **2024**, *14*, 5032. [CrossRef] [PubMed]

29. Del Pizzo, A.; Di Noia, L.P.; Meo, S. Super twisting sliding mode control of smart-inverters grid-connected for PV applications. In Proceedings of the 2017 IEEE 6th International Conference on Renewable Energy Research and Applications (ICRERA), San Diego, CA, USA, 5–8 November 2017; pp. 793–796.

30. Khare, A.; Rangnekar, S. A review of particle swarm optimization and its applications in solar photovoltaic system. *Appl. Soft Comput.* **2013**, *13*, 2997–3006. [CrossRef]

31. Kumar, D.; Chatterjee, K. A review of conventional and advanced MPPT algorithms for wind energy systems. *Renew. Sustain. Energy Rev.* **2016**, *55*, 957–970. [CrossRef]